Journal of Inorganic Biochemistry 204 (2020) 110959

Contents lists available at ScienceDirect

Journal of Inorganic Biochemistry

journal homepage: www.elsevier.com/locate/jinorgbio

Urease inhibition studies of six Ni(II), Co(II) and Cu(II) complexes with two sexidentate N_2O_4-donor bis-Schiff base ligands: An experimental and DFT computational study

Hu Wang[a], Cungang Xu[a], Xia Zhang[a], Dongmei Zhang[a], Fan Jin[b,*], Yuhua Fan[a,*]

[a] Key Laboratory of Marine Chemistry Theory and Technology, Ministry of Education, College of Chemistry and Chemical Engineering, Ocean University of China, Qingdao, China

[b] HITS-Heidelberg Institute for Theoretical Studies, Schloß Wolfsbrunnenweg 35, 69118 Heidelberg, Germany

ARTICLE INFO

Keywords:
Metal complex
X-ray structure
Theoretical calculation
Urease inhibitor
Molecular docking

ABSTRACT

Six novel complexes, $[Ni(C_{36}H_{34}N_2O_{10})]\cdot 2.25CH_3OH\cdot 0.5C_4H_{10}O$ (**1**), $[Co(C_{36}H_{34}N_2O_{10})]$ (**2**), $[Cu(C_{36}H_{34}N_2O_{10})]\cdot 2CH_3OH$ (**3**), $[Ni(C_{36}H_{32}N_2O_8Cl_2)]\cdot 2CH_3OH$ (**4**), $[Co(C_{36}H_{32}N_2O_8Cl_2)]\cdot 4CH_3OH$ (**5**) and $[Cu(C_{36}H_{32}N_2O_8Cl_2)]\cdot 2CH_3OH$ (**6**) with two sexidentate N_2O_4-donor bis-Schiff base ligands ($C_{36}H_{34}N_2O_{10}$ = 1,2-bis(2-methoxy-6-formylphenoxy)ethane-L-tyrosine; $C_{36}H_{32}N_2O_8Cl_2$ = 1,2-bis(2-methoxy-6-formylphenoxy)ethane-L-4-chlorophenylalanine) have been synthesized and structurally characterized. Theoretical calculation of the six complexes was carried out by density functional theory (DFT) Becke's three-parameter hybrid (B3LYP) method employing the 6-3lG basis set, indicating that the calculation results are in accordance with experimental results. Moreover, the inhibitory activities of complexes **1**–**6** were tested in vitro against jack bean urease. At the same time, molecular docking was investigated to determine the probable binding mode. The experimental values and docking simulation exhibited that complexes **3** and **6** showed strong inhibitory activity (IC_{50} = 10.36 ± 1.13, 15.63 ± 3.04 μM) compared with the positive reference acetohydroxamic acid (IC_{50} = 26.99 ± 1.43 μM). Their structure-inhibitory activity relationship was further discussed from the perspective of molecular docking and theoretical calculation.

1. Introduction

In the past few decades, the research of pharmaceutical inorganic chemistry has developed rapidly. Metal complexes have various important therapeutic applications in different areas, such as cancer treatment [1–5], antibacterial therapy [6–8], and anti-inflammatory agents [9–11]. The metallodrugs play an important role in the process of enzyme inhibition due to their unique mode of interaction compared with common organic inhibitor. The metal ion is the key of the good inhibitory activities of metal complexes and the activities are mainly influenced by coordination environment of the metal ion and its oxidation state as well as of the structure of the ligand [12–19]. It's worth noting that Schiff base complexes have gained considerable attention due to their remarkable biological activities (such as, antibacterial, anti-inflammatory and antiviral activities) [20,21,22,23], catalytic activities [24–26], electroluminescent properties [27,28], fluorescence properties [29], nonlinear optical (NLO) properties [30], and applications in sensors [31] and organic photovoltaic materials [32].

Urease is implicated in the pathogenesis of a number of human pathogens, including bacteria Yersinia enterocolitica, *Proteus mirabilis* and *Mycobacterium tuberculosis* [33–35]. Another major ureolytic pathogen is Helicobacter pylori, the originator of several severe disease conditions, such as gastritis, gastric ulcers or even gastric cancer [36–38]. Urease inhibitors have long been considered as targets for new antiulcer drugs, as the ureolytic activity of the bacterial pathogens results in damage to gastric epithelium, leading to inflammation [34]. Recently, urease inhibition study has attracted increasing attention [39–42] and numerous of Schiff base complexes' inhibitory activities have been detected due to their good inhibitory performance [43–46].

To the best of our knowledge, there is rare report on the synthesis of two different series of Ni(II), Co(II) and Cu(II) complexes with sexidentate N_2O_4-donor bis-Schiff base ligand and the study of structure-urease inhibitory activity relationship discussed from the perspective of molecular docking and theoretical calculation. In view of these observations, in this work, six novel complexes, $[Ni(C_{36}H_{34}N_2O_{10})]\cdot 2.25CH_3OH\cdot 0.5C_4H_{10}O$ (**1**), $[Co(C_{36}H_{34}N_2O_{10})]$ (**2**),

* Corresponding authors.
E-mail addresses: pkujinfan@gmail.com (F. Jin), haidafyh301@163.com (Y. Fan).

https://doi.org/10.1016/j.jinorgbio.2019.110959
Received 27 October 2019; Received in revised form 3 December 2019; Accepted 9 December 2019
Available online 16 December 2019
0162-0134/

$[Cu(C_{36}H_{34}N_2O_{10})]\cdot 2CH_3OH$ (**3**), $[Ni(C_{36}H_{32}N_2O_8Cl_2)]\cdot 2CH_3OH$ (**4**), $[Co(C_{36}H_{32}N_2O_8Cl_2)]\cdot 4CH_3OH$ (**5**) and $[Cu(C_{36}H_{32}N_2O_8Cl_2)]\cdot 2CH_3OH$ (**6**) with two sexidentate N_2O_4-donor bis-Schiff base ligands ($C_{36}H_{34}N_2O_{10}$ = 1,2-bis(2-methoxy-6-formylphenoxy)ethane-L-tyrosine; $C_{36}H_{32}N_2O_8Cl_2$ = 1,2-bis(2-methoxy-6-formylphenoxy)ethane-L-4-chlorophenylalanine) have been synthesized, characterized and evaluated in the urease inhibitory activity. Additionally, based on crystal data, density functional theory (DFT) calculation of six complexes was performed using the Gaussian 03 program suite. Nevertheless, due to the interest of understanding their role in urease inhibition, docking simulation was carried out using the AutoDock Vina program to position the complex into the active site of urease to determine the probable binding mode. The docking result show good correlation with experimental data. At last, the structure-inhibitory activity relationship was further discussed from the perspective of molecular docking and theoretical calculation.

2. Experimental

2.1. Chemicals and physical measurements

All chemical reagents were of analytical grade and were used without further purification. L-tyrosine and L-4-chlorophenylalanine were purchased from Aladdin. Urease (from jack beans, type III, activity 31,660 units/mg solid), *N*-[2-hydroxyethyl]piperazine-*N*′-[2-ethanesulfonic acid] (HEPES) buffer and urea (Molecular Biology Reagent) were purchased from Sigma-Aldrich Co. (St. Louis, MO, USA). IR spectra were recorded as KBr pellets on a Nicolet 170SX spectrophotometer in the 4000–400 cm^{-1} region. Elemental analyses (C, H and N) were obtained with a model 2400 Perkin-Elmer analyzer. X-ray diffraction data were collected on an Enraf-nonius CAD-4 diffractometer. Enzyme inhibitory activity was measured with a BioTek Synergy HT microplate reader.

2.2. Synthesis of the complexes

$[Ni(C_{36}H_{34}N_2O_{10})]\cdot 2.25CH_3OH\cdot 0.5C_4H_{10}O$ (**1**): L-tyrosine (0.181 g, 1.0 mmol) and potassium hydroxide (0.056 g, 1.0 mmol) were dissolved in methanol (40 mL) and then 1,2-bis(2-methoxy-6-formylphenoxy)ethane (0.165 g, 0.5 mmol) [47] was added to the solution. The mixture was heated to 50 °C with stirring and then refluxed for 5 h to give a bright yellow solution. After that, a methanol solution (15 mL) of $Ni(CH_3COO)_2\cdot 4H_2O$ (0.124 g, 0.5 mmol) was added to the above solution. The resulting mixture was stirred and refluxed at 50 °C for 5 h. The resulting solution was cooled at room temperature and then filtered. The dark green block-shaped crystals were formed after about 4 days by slow diffusion of ether into a concentrated methanol solution of the complex at room temperature. Yield: 63% based on L-tyrosine. IR (KBr, cm^{-1}): 1647, 1578, 1364, 1197, 551, 448. Elemental Anal Calc (%) for $[Ni(C_{36}H_{34}N_2O_{10})]\cdot 2.25CH_3OH\cdot 0.5C_4H_{10}O$: C 58.77, H 5.88, N 3.41; found: C 58.65, H 6.02, N 3.52.

$[Co(C_{36}H_{34}N_2O_{10})]$ (**2**): The complex was synthesized by a procedure similar to that for the complex **1**, but using $Co(CH_3COO)_2\cdot 4H_2O$ (0.125 g, 0.5 mmol) instead of $Ni(CH_3COO)_2\cdot 4H_2O$. The red block-shaped crystals were formed after about 3 days by slow diffusion of ether into a concentrated methanol solution of the complex at room temperature. Yield: 66% based on L-tyrosine. IR (KBr, cm^{-1}): 1644, 1579, 1362, 1202, 557, 452. Elemental Anal Calc (%) for $[Co(C_{36}H_{34}N_2O_{10})]$: C 60.59, H 4.80, N 3.93; found: C 60.46, H 4.92, N 4.03.

$[Cu(C_{36}H_{34}N_2O_{10})]\cdot 2CH_3OH$ (**3**): The complex was synthesized by a procedure similar to that for the complex **1**, but using $Cu(CH_3COO)_2\cdot H_2O$ (0.125 g, 0.5 mmol) instead of $Ni(CH_3COO)_2\cdot 4H_2O$. The filtrate was left for slow evaporation at room temperature. The blue block-shaped crystals were formed after about 1 week. Yield: 65% based on L-tyrosine. IR (KBr, cm^{-1}): 1649, 1581, 1379, 1215, 554, 459. Elemental Anal Calc (%) for $[Cu(C_{36}H_{34}N_2O_{10})]\cdot 2CH_3OH$: C 58.34, H 5.41, N 3.58; found: C 58.15, H 5.69, N 3.64.

$[Ni(C_{36}H_{32}N_2O_8Cl_2)]\cdot 2CH_3OH$ (**4**): The complex was synthesized by a procedure similar to that for the complex **1**, but using L-4-chlorophenylalanine (0.100 g, 0.5 mmol) instead of L-tyrosine. The dark green block-shaped crystals were formed after about 3 days by slow diffusion of ether into a concentrated methanol solution of the complex at room temperature. Yield: 62% based on L-4-chlorophenylalanine. IR (KBr, cm^{-1}): 1654, 1575, 1356, 1206, 550, 456. Elemental Anal Calc (%) for $[Ni(C_{36}H_{32}N_2O_8Cl_2)]\cdot 2CH_3OH$: C 56.05, H 4.95, N 3.44; found: C 55.91, H 5.08, N 3.50.

$[Co(C_{36}H_{32}N_2O_8Cl_2)]\cdot 4CH_3OH$ (**5**): The complex was synthesized by a procedure similar to that for the complex **4**, but using $Co(CH_3COO)_2\cdot 4H_2O$ (0.125 g, 0.5 mmol) instead of $Ni(CH_3COO)_2\cdot 4H_2O$. The red block-shaped crystals were formed after about 3 days by slow diffusion of ether into a concentrated methanol solution of the complex at room temperature. Yield: 63% based on L-4-chlorophenylalanine. IR (KBr, cm^{-1}): 1648, 1577, 1363, 1210, 546, 459. Elemental Anal Calc (%) for $[Co(C_{36}H_{32}N_2O_8Cl_2)]\cdot 4CH_3OH$: C 54.68, H 5.51, N 3.19; found: C 54.57, H 5.61, N 3.25.

$[Cu(C_{36}H_{32}N_2O_8Cl_2)]\cdot 2CH_3OH$ (**6**): The complex was synthesized by a procedure similar to that for the complex **4**, but using $Cu(CH_3COO)_2\cdot H_2O$ (0.125 g, 0.5 mmol) instead of $Ni(CH_3COO)_2\cdot 4H_2O$. The blue block-shaped crystals were formed after about 4 days by slow diffusion of ether into a concentrated methanol solution of the complex at room temperature. Yield: 65% based on L-4-chlorophenylalanine. IR (KBr, cm^{-1}): 1653, 1580, 1379, 1209, 561, 457. Elemental Anal Calc (%) for $[Cu(C_{36}H_{32}N_2O_8Cl_2)]\cdot 2CH_3OH$: C 55.71, H 4.92, N 3.42; found: C 55.59, H 5.12, N 3.53.

2.3. Crystallographic data collection and structure determination

Single crystals with dimensions of 0.3 × 0.22 × 0.15 (**1**), 0.28 × 0.15 × 0.12 (**2**), 0.28 × 0.15 × 0.12 (**3**), 0.28 × 0.15 × 0.12 (**4**), 0.19 × 0.15 × 0.12 (**5**), 0.19 × 0.15 × 0.12 mm (**6**) were mounted on a Bruker APEX-II CCD X-ray single-crystal diffractometer at 173 K with graphite-monochromatized Mo-Kα radiation (λ = 0.71073 Å) by using the φ and ω scan mode at room temperature. SADABS2008/1 is applied to absorption correction. The structures were solved and refined by using SHELXT and SHELX [48] programs. Choose the highest symmetry in all cases. Derivation of non-hydrogen atoms by Fourier synthesis. The positional and thermal parameters were refined by full matrix least-squares (on F^2) to convergence [49]. The hydrogen atom of the organic ligand is theoretically determined and improved by a fixed thermal factor.

2.4. Computational procedure

Becke's three-parameter hybrid (B3LYP) level was selected for DFT calculation by the basis set of 6-31G for the C, H, O, N and Cl atoms [50–52], while LANL2DZ basis set was used for Ni, Co and Cu atoms [53]. Atom coordinates used in the calculations were from crystallographic data, and a molecule in the unit cells was selected as the initial model. All calculations were conducted on a Pentium IV computer using Gaussian 03 program [54].

2.5. Measurement of jack bean urease inhibitory activity

The measurement of urease activity was carried out according to the literature reported by Tanaka [55]. Generally, the assay mixture, containing 25 μL of jack bean urease (40 kU/L) (dissolved in distilled water) and 25 μL of the tested complexes with different concentrations (dissolved in DMSO/H_2O mixture (1:1 v/v)), was preincubated for 1 h at 37 °C in a 96-well assay plate. After preincubation, 200 μL of 100 mmol HEPES (*N*-[2-hydroxyethyl]piperazine-*N*′-[2-ethanesulfonic acid]) buffer pH = 6.8 containing 500 mmol urea and 0.002% phenol

red were added and incubated at 37 °C [56]. The reaction was measured by micro plate reader (570 nm), which was required to produce enough ammonium carbonate to raise the pH of a HEPES buffer from 6.8 to 7.7, the endpoint being determined by the colour of phenol red indicator [57].

2.6. Docking simulations

Molecular docking of the inhibitor with the three-dimensional structure of jack bean urease was carried out using the AutoDock Vina program suite [58]. The ligand structure in docking protocol was used as a crystal structure. The crystal structure of jack bean urease was obtained from Protein Data Bank (http://www.pdb.org/pdb/home/home.do) with the PDB ID of 3LA4 at a resolution of 2.05 Å. The graphical user interface AutoDockTools (ADT 1.5.4) was performed to setup every inhibitor enzyme interaction where all hydrogen atoms were added, Gasteiger charges were calculated and nonpolar hydrogen atoms were merged to carbon atoms. In all docking, a grid box with a size of 60 Å pointing in x, y and z directions was centered on the catalytic site of the protein. The docking parameters were set to default. The flexible ligand mode was used for docking. The docking procedure of the complexes **1–6** with the active site of jack bean urease was performed as described.

3. Results and discussion

3.1. Synthesis

The general synthesis of the complexes **1–6** is shown in Scheme 1. In the first step, 1,2-bis(2-methoxy-6-formylphenoxy)ethane was synthesized by the reaction between o-vanillin and 1,2-dibromoethane with the ratio of 2:1. Then, 1,2-bis(2-methoxy-6-formylphenoxy)ethane reacted with L-tyrosine and L-4-chlorophenylalanine respectively to form the corresponding N_2O_4-donor bis-Schiff base. Finally, two types of bis-Schiff bases reacted with $Ni(CH_3COO)_2{\cdot}4H_2O$, $Co(CH_3COO)_2{\cdot}4H_2O$ and $Cu(CH_3COO)_2{\cdot}H_2O$ respectively with the ratio of 1:1 to afford the complexes **1–6**. Crystals of complexes **1–6** suitable for X-ray diffraction can be obtained through slow evaporation method and liquid-liquid diffusion method. The summary of the key crystallographic information are given in Table 1 and Table 2.

3.2. Crystal structure description

The molecular structures of complexes **1–6** were determined by single crystal X-ray analysis as shown in Figs. 1-6, and the comparison of the selected bond lengths and angles of the complexes can be found in Table S1 and Table S2.

3.2.1. Crystal structure of $[Ni(C_{36}H_{34}N_2O_{10})]{\cdot}2.25CH_3OH{\cdot}0.5C_4H_{10}O$ (1)

Complex **1** crystallizes in the orthorhombic crystal system and space group $P2_12_12_1$ (Table 1). As shown in Fig. 1a, the central Ni(II) adopts a distorted octahedral geometry that is defined by two nitrogen donors from C═N groups occupying the axial positions, two oxygen donors from ether groups and two oxygen donors from carboxyl groups in the equatorial plane, forming a type of sexidentate N_2O_4-donor bis-Schiff base complex.

The corresponding bond angles of O(3)—Ni(1)—O(6) [166.22 (14)°] and O(4)—Ni(1)—O(7) [164.79 (14)°] are both less than 180° apparently, while, the bond angle of N(1)—Ni(1)—N(2) [174.48 (18)°] is very close to 180°. At the same time, the bond angles of N(1)—Ni(1)—O(3) [83.11 (16)°], N(1)—Ni(1)—O(4) [94.68 (15)°], N(1)—Ni(1)—O(6) [78.01 (14)°] and N(1)—Ni(1)—O(7) [97.88 (16)°] indicate that the central Ni(II) adopts a distorted octahedral geometry. Atoms O(3), O(4), O(6) and O(7) occupy each vertex of the basal site, while N(1) and N(2) locate in the apical positions of the octahedral structure. The bond lengths of N(1)—C(10) and N(2)—C(26) are 1.267 (7) and 1.262 (7) Å respectively, which are consistent with our previous reported values [46,59,60]. It indicates that there are two double bonds in this complex: the first between C(10) and N(1), and the other between C(26) and N(2). The bond lengths of Ni(1)—O(3) and Ni(1)—O(4) are 1.993 (4) Å and 2.012 (4) Å respectively, which are shorter than those of Ni(1)—O(6) 2.104 (4) Å and Ni(1)—O(7) 2.097 (3) Å, suggesting that the coordination abilities of the carboxyl O(3) and O(4) are stronger than those of the ether O(6) and O(7) atoms (Table S1). Furthermore, each ligand serves as a bridging ligand to connect two Ni(II) centers into supramolecular by O—H···O hydrogen bonds (yellow dash bonds: O(1)—H(1)···O(4), symmetry code: x − 1/2, −y + 3/2, −z + 1) and C—H···O interactions (red dash bonds), forming a two dimensional supramolecular layer structure (Fig. 1b, Table S3).

3.2.2. Crystal structure of $[Co(C_{36}H_{34}N_2O_{10})]$ (2)

Complex **2** crystallizes in the orthorhombic crystal system and space group $P2_12_12_1$. The complex also has a distorted octahedral geometry in which the carboxyl O atoms are also more tightly coordinated than the ether O atoms (Fig. 2a, Table S1). The 2-D structure of complex **2** is formed by two types of O—H···O hydrogen bonds (yellow dash bonds: O(8)—H(8)···O(2), symmetry code: 1/2+x, 1/2-y, 1-z; O(10)—H(10)···O(3), symmetry code: 1 − x, 1/2 + y, 1/2 − z) and C—H···O interactions (red dash bonds) (Fig. 2b, Table S3).

3.2.3. Crystal structure of $[Cu(C_{36}H_{34}N_2O_{10})]{\cdot}2CH_3OH$ (3)

Complex **3** crystallizes in the orthorhombic crystal system and space group $P2_12_12_1$. The complex also has a distorted octahedral geometry in which the carboxyl O atoms are also more tightly coordinated than the ether O atoms (Fig. 3a, Table S1). In addition, there is two free solvent methanol molecules in the crystalline lattice. The 2-D structure of

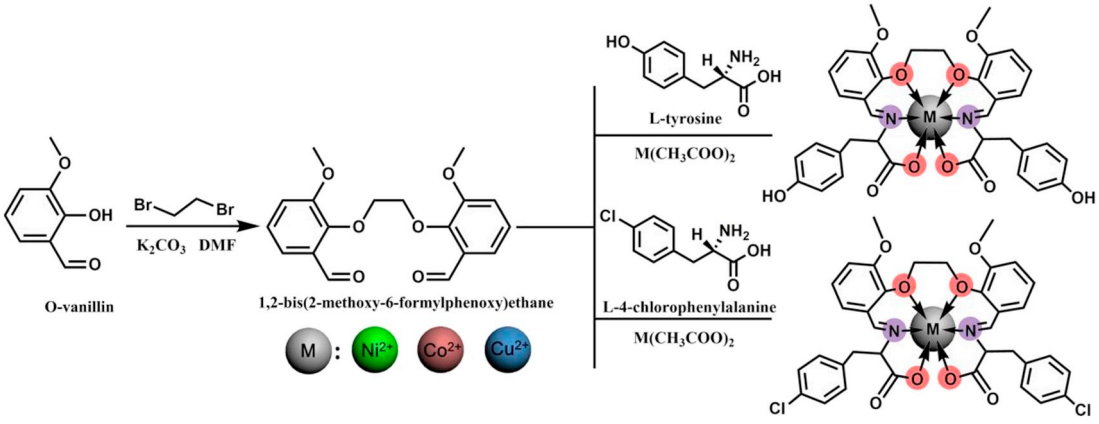

Scheme 1. The general synthesis routes of six complexes **1–6**.

Table 1
Crystal data and structure refinement parameters for complexes **1–3**.

Parameter	1	2	3
Empirical formula	$C_{40.25}H_{48}N_2O_{12.75}Ni$	$C_{36}H_{34}N_2O_{10}Co$	$C_{38}H_{42}N_2O_{12}Cu$
Formula weight	822.51	713.58	782.27
Temperature (K)	170	173	205
Wavelength (Å)	0.71073	0.71073	0.71073
Crystal system	Orthorhombic	Orthorhombic	Orthorhombic
Space group	$P2_12_12_1$	$P2_12_12_1$	$P2_12_12_1$
a (Å)	11.236 (4)	11.145 (4)	12.647 (3)
b (Å)	11.621 (5)	11.625 (5)	16.476 (3)
c (Å)	37.220 (17)	38.061 (15)	8.8918 (18)
α (°)	90	90	90
β (°)	90	90	90
γ (°)	90	90	90
Volume (Å^3)	4860 (4)	4931 (3)	1852.7 (6)
Z	4	4	2
Calculated density (g/cm^3)	1.124	0.961	1.402
Absorption coefficient (mm^{-1})	0.454	0.390	0.656
F(000)	1734	1484	818
Crystal size (mm)	0.3 × 0.22 × 0.15	0.28 × 0.15 × 0.12	0.28 × 0.15 × 0.12
θ range for data collection (°)	1.836 to 27.817	1.070 to 25.007	2.030 to 27.586
Limiting indices	$-12 \le h \le 14$	$-11 \le h \le 13$	$-16 \le h \le 16$
	$-15 \le k \le 15$	$-13 \le k \le 13$	$-19 \le k \le 21$
	$-46 \le l \le 48$	$-45 \le l \le 43$	$-11 \le l \le 11$
Reflections collected/unique	25,108/11,376	31,961/8678	15,413/4263
	[R_{int} = 0.0547]	[R_{int} = 0.1263]	[R_{int} = 0.064]
Completeness to θ = 25.02	0.990	0.998	0.994
Max. and min. Transmission	0.7456 and 0.5786	0.7452 and 0.5671	0.7456 and 0.6184
Data/restraints/parameters	11,376/532/558	8678/480/411	4263/0/244
Goodness of fit on F^2	1.094	0.975	1.019
R_1[a], wR_2[b] [$I > 2\sigma(I)$]	R_1 = 0.0798	R_1 = 0.0955	R_1 = 0.0477
	wR_2 = 0.2080	wR_2 = 0.2437	wR_2 = 0.1026
R_1[a], wR_2[b] (all data)	R_1 = 0.1003	R_1 = 0.1398	R_1 = 0.0671
	wR_2 = 0.2201	wR_2 = 0.2630	wR_2 = 0.1120
Largest diff. peak and hole (e. Å^3)	0.757 and −0.629	0.806 and −0.512	0.566 and −0.530

[a] $R = \Sigma(|F_0|\text{-}|F_C|)/\Sigma|F_0|$.
[b] $wR = [\Sigma w(|F_0|^2\text{-}|F_C|^2)^2/\Sigma w(F_0^2)]^{1/2}$.

complex **3** is formed by two types of O—H···O hydrogen bonds (yellow dash bonds: O(5)—H [5]···O [6], symmetry code: x − 1, y, z; O(6)—H (6A)···O [3], symmetry code: -) and C—H···O interactions (red dash bonds) (Fig. 3b, Table S3).

3.2.4. Crystal structure of [Ni($C_{36}H_{32}N_2O_8Cl_2$)]·2CH_3OH (4)

Complex **4** crystallizes in the orthorhombic crystal system and space group $P2_12_12_1$. The complex also has a distorted octahedral geometry in which the carboxyl O atoms are also more tightly coordinated than the ether O atoms (Fig. 4a, Table S2). In addition, there is two free solvent methanol molecules in the crystalline lattice. The 2-D structure of complex **4** is constructed by C—H···O interactions (red dash bonds). (Fig. 4b).

3.2.5. Crystal structure of [Co($C_{36}H_{32}N_2O_8Cl_2$)]·4CH_3OH (5)

Complex **5** crystallizes in the monoclinic crystal system and space group $C2/c$. The complex also has a distorted octahedral geometry in which the carboxyl O atoms are also more tightly coordinated than the ether O atoms (Fig. 5a, Table S2). In addition, there is four free solvent methanol molecules in the crystalline lattice. The 2-D structure of complex **5** is constructed by one type of O—H···O hydrogen bonds (yellow dash bonds: O(6)—H [6]—O [1], symmetry code: -) and C—H···O interactions (red dash bonds) (Fig. 5b, Table S3).

3.2.6. Crystal structure of [Cu($C_{36}H_{32}N_2O_8Cl_2$)]·2CH_3OH (6)

Complex **6** crystallizes in the orthorhombic crystal system and space group $P2_12_12$. The complex also has a distorted octahedral geometry in which the carboxyl O atoms are also more tightly coordinated than the ether O atoms (Fig. 6a, Table S2). In addition, there is two free solvent methanol molecules in the crystalline lattice. The 2-D structure of complex **6** is formed by one type of O—H···O hydrogen bonds (yellow dash bonds: O(3)—H(3)···O(2), symmetry code: -), C—H···O interactions (red dash bonds) and C—H···Cl interactions (dark-red dash bonds) (Fig. 6b, Table S3).

3.3. DFT calculations

In the present study, the superposition of optimized (fuchsia) and crystal structures (turquoise) of complexes **1–6** are depicted in Fig. S1 and Fig. S2. It is clear that the coordination environment part of each complex is well superimposed together. This proves that the selected basis sets are suitable for the calculation of complexes **1–6**.

As we know, molecular electrostatic potential (MEP) is related to the electronic density and is a very useful descriptor in understanding sites for electrophilic attack and nucleophilic reactions [61]. The electrostatic potential V(r) is also well suited for analyzing processes based on the 'recognition' of one molecule by another, as in drug-receptor and enzyme-substrate interactions, in which two species first 'see' each other through their potentials [62]. To predict the electrophilic or nucleophilic attack sites, molecule 'recognition' sites and hydrogen bonding or weak interactions for the investigated molecules, MEP surfaces were obtained based on the optimized geometry.

Herein, only the MEP maps of optimized structures of complexes **3** and **6** (Fig. 7) were discussed as an example because the MEP maps of other complexes are very similar by judging from the Figs. S9–S12, and the MEP interval distributions [63,64] of complexes **3** and **6** were depicted in Fig. 8. The surface area distribution in different electrostatic potential intervals of the two complexes is relatively even. For complex **3**, the percentage of positive and negative electrostatic potential areas are 47.64% and 52.36% respectively. For complex **6**, the percentage of positive and negative electrostatic potential areas are 44.88% and 55.12% respectively. It is clear that the most positive regions are

Table 2
Crystal data and structure refinement parameters for complexes **4–6**.

Parameter	4	5	6
Empirical formula	$C_{38}H_{40}N_2O_{10}Cl_2Ni$	$C_{40}H_{48}N_2O_{12}Cl_2Co$	$C_{38}H_{40}N_2O_{10}Cl_2Cu$
Formula weight	814.33	878.63	819.16
Temperature (K)	173	173	173
Wavelength (Å)	0.71073	0.71073	0.71073
Crystal system	Orthorhombic	Monoclinic	Orthorhombic
Space group	$P2_12_12_1$	$C2/c$	$P2_12_12$
a (Å)	14.347 (5)	19.967 (4)	13.437 (2)
b (Å)	16.728 (5)	10.5685 (18)	15.501 (3)
c (Å)	16.853 (6)	20.021 (4)	9.0373 (14)
α (°)	90	90	90
β (°)	90	101.294 (6)	90
γ (°)	90	90	90
Volume (Å^3)	4045 (2)	4143.1 (13)	1882.4 (5)
Z	4	4	2
Calculated density (g/cm^3)	1.337	1.409	1.445
Absorption coefficient (mm^{-1})	0.668	0.607	0.782
F(000)	1696	1836	850
Crystal size (mm)	0.28 × 0.15 × 0.12	0.19 × 0.15 × 0.12	0.19 × 0.15 × 0.12
θ range for data collection (°)	1.715 to 26.407	2.075 to 25.008	2.006 to 26.363
Limiting indices	$-14 \le h \le 17$ $-20 \le k \le 20$ $-21 \le l \le 21$	$-23 \le h \le 23$ $-12 \le k \le 12$ $-23 \le l \le 22$	$-15 \le h \le 16$ $-19 \le k \le 19$ $-10 \le l \le 11$
Reflections collected/unique	33,211/8284 [R_{int} = 0.0874]	15,267/3667 [R_{int} = 0.1070]	8026/3657 [R_{int} = 0.0897]
Completeness to θ = 25.02	0.998	0.999	0.965
Max. and min. transmission	0.7454 and 0.6602	0.7455 and 0.6174	0.7140 and 0.4699
Data/restraints/parameters	8284/0/485	3667/0/263	3657/0/243
Goodness of fit on F^2	0.988	0.982	0.988
R_1[a], wR_2[b] [$I > 2\sigma(I)$]	R_1 = 0.0466 wR_2 = 0.0931	R_1 = 0.0571 wR_2 = 0.1213	R_1 = 0.0627 wR_2 = 0.1093
R_1[a], wR_2[b] (all data)	R_1 = 0.0752 wR_2 = 0.1047	R_1 = 0.1005 wR_2 = 0.1387	R_1 = 0.1083 wR_2 = 0.1319
Largest diff. peak and hole (e. Å^3)	0.437 and −0.424	0.689 and −0.439	0.427 and −0.314

[a] $R = \Sigma(|F_0|\text{-}|F_C|)/\Sigma|F_0|$.
[b] $wR = [\Sigma w(|F_0|^2\text{-}|F_C|^2)^2/\Sigma w(F_0^2)]^{1/2}$.

located around hydroxyl oxygens (yellow ball, V(r): 0.079 a.u., 0.079 a.u.) of the complexes **3**, indicating that these atoms are possible sites for nucleophilic attack. In contrast, the most negative regions are located around carboxyl oxygens (magenta ball, V(r): −0.097 a.u., −0.097 a.u.; −0.093 a.u., −0.094 a.u.) of the complexes **3** and **6**. Thus, these atoms are preferred possible sites for electrophilic attack. At the same time, these hydroxyl oxygens and carboxyl oxygens may form hydrogen bond or weak interaction. It is consistent with the experimental results that hydroxyl oxygens and carboxyl oxygens are proton donors and receptors of hydrogen bonds respectively, through which the supermolecular structure is assembled (Figs. 1b-6b; Table S3). The hydroxyl oxygens and the carboxyl oxygens with the extreme values of the electrostatic potential may be the first to be seen in the molecular recognition process or enzyme-substrate interaction process.

At the same time, the discussion of the natural atomic charges and frontier molecular orbitals can be found in Supplementary Information (SI) file (Tables S4–S7, Figs. S3–S8).

3.4. Inhibitory activity against jack bean urease

Two Schiff base ligands and the corresponding Ni(II), Co(II) and Cu (II) complexes **1–6** were screened for inhibitory activity against jack bean urease (Table 3). It was found that the synthesized ligands H_2L_{1-2} exhibited no inhibitory ability to inhibit the jack bean urease.

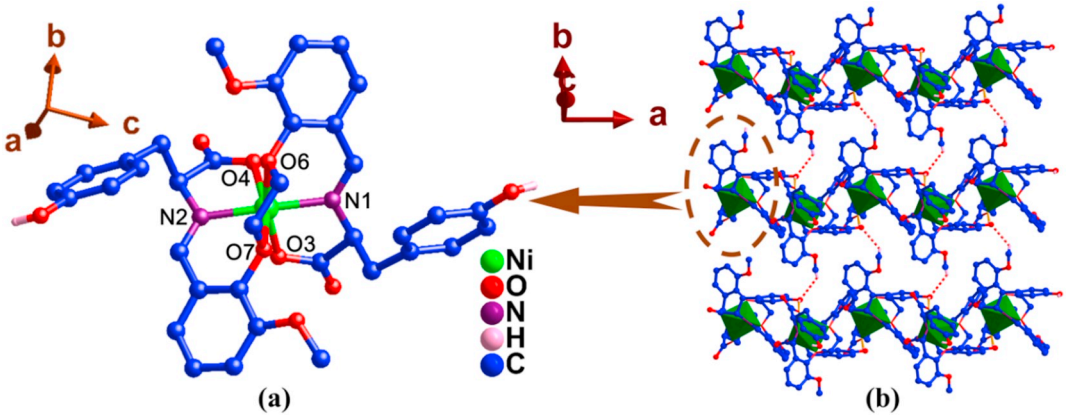

Fig. 1. The molecular structure (a) and the 2-D layer structure (b) of $[Ni(C_{36}H_{34}N_2O_{10})]\cdot 2.25CH_3OH\cdot 0.5C_4H_{10}O$ (**1**), which constructed by O—H···O hydrogen bonds (yellow dash bonds) and C—H···O interactions (red dash bonds).

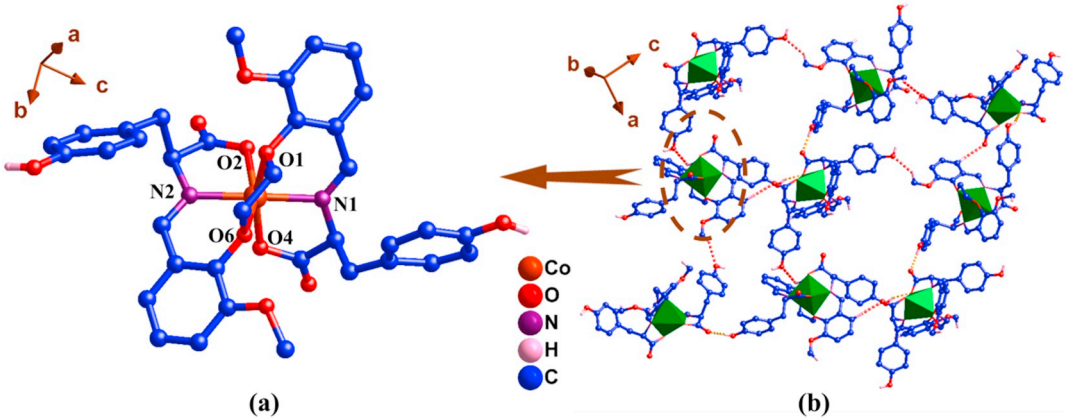

Fig. 2. The molecular structure (a) and the 2-D layer structure (b) of [Co($C_{36}H_{34}N_2O_{10}$)] (**2**), which constructed by O—H···O hydrogen bonds (yellow dash bonds) and C—H···O interactions (red dash bonds).

Compared with the standard inhibitor acetohydroxamic acid (AHA, IC_{50} = 26.99 ± 1.43 μM), the Schiff base complexes **3** and **6** displayed potent inhibitory activity (IC_{50} = 10.36 ± 1.13; 15.63 ± 3.04 μM). Thus it can be seen that coordination to Cu(II) ion resulted in the improved inhibitory activity [65–67]. It should be noted that in terms of the inhibitory strength towards jack bean urease the complexes studied form the order: **3** > **6** > **1** > **2** > **4** > **5**. Interestingly, complex **3** is potent than complex **6** as a result of the difference between electron-giving substituent (hydroxy) and electron-withdrawing substituent (chlorine) on the aromatic ring. At the same time, the spatial steric hindrance of the 4-chlorophenyl pendant group in complex **6** is higher than that of the 4-hydroxyphenyl pendant group in complex **3**. When compared with Cu(II) complexes **3** and **6**, the Ni(II) and Co(II) complexes (**1**, **2**, **4** and **5**) exhibit weaker urease inhibitory activity under the same condition. The results indicate that inhibitory activities of metal complexes as the urease inhibitor depend on not only the organic ligands but also the central ions [66].

3.5. Molecular docking study

The binding models of complexes **1**, **3**, **4** and **6** with jack bean urease (3LA4) were simulated using the AutoDock Vina program [58] to validate their structure-activity relationships. The results revealed that the four target molecules fitted well in the active pocket of jack bean urease (Fig. S13). Additional interactions were established in a variety of conformations because of the flexibility of the complexes and the amino acid residues of the urease. The optimized cluster (10 occurrences) was ranked by energy level in the best conformation of the inhibitor-urease modeled structures, and the affinity energy of the amino acid residues with the corresponding M(II) complexes **1**, **3**, **4** and **6** showed −37.24, −41.42, −36.00 and −39.33 kJ/mol respectively. The docking results further verify the difference of their urease inhibitory activities obtained from the urease-inhibitory measurement.

The binding models of complexes **1**, **3**, **4** and **6** with urease (3LA4) were shown in Fig. 9, Fig. 10, Fig. S14 and Fig. S15, with all the amino acid residues that interact with urease indicated. In the binding model, the carboxyl O atom of complex **1** forms one hydrogen bond with the side chain N—H of MET746 with the distance and angle of the N—⊖H···$O_{complex\text{-}1}$ being 2.085 Å and 139.5° respectively. The phenolic H atom of complex **1** forms one hydrogen bond with the O atom of GLY12. The hydrogen-bonding distance and angle of O—$H_{complex\text{-}1}$···O_{GLY12} are 1.911 Å and 155.4°. At the same time, complex **1** formed cation-π interaction with said chain N cation of amino-acid residue LYS716, with the distance of the interaction being 6.214 Å (Fig. S14a). Notably, in the best docking conformation (Fig. 9a), as expected, complex **3** formed three types of hydrogen bonds with amino-acid residues MET746, LEU839 and SER421. The hydrogen-bonding distances and angles of MET746 N—H···$O_{complex\text{-}3}$, LEU839 N—H···$O_{complex\text{-}3}$ and complex-3 O—H···O_{SER421} are 2.451, 2.322, 2.347 Å and 107.2, 172.5, 106.5° respectively. The carboxyl O atom of complex **4** forms one hydrogen bond with the side chain O—H of SER834 with the distance and angle of the interaction being 2.269 Å and 124.6° respectively. The methoxy O atom complex **4** forms one hydrogen bond with the side chain O—H of THR578 with the distance and angle of the interaction being 2.309 Å and 162.2° respectively (Fig. S15a). The two carboxyl O atoms of complex **6** forms one hydrogen bond with the side chain N—H of MET746 and N—H of LEU839 respectively. The hydrogen-bonding distance and angle of MET746 N—H···$O_{complex\text{-}6}$ are 2.240 Å and 110.4°,

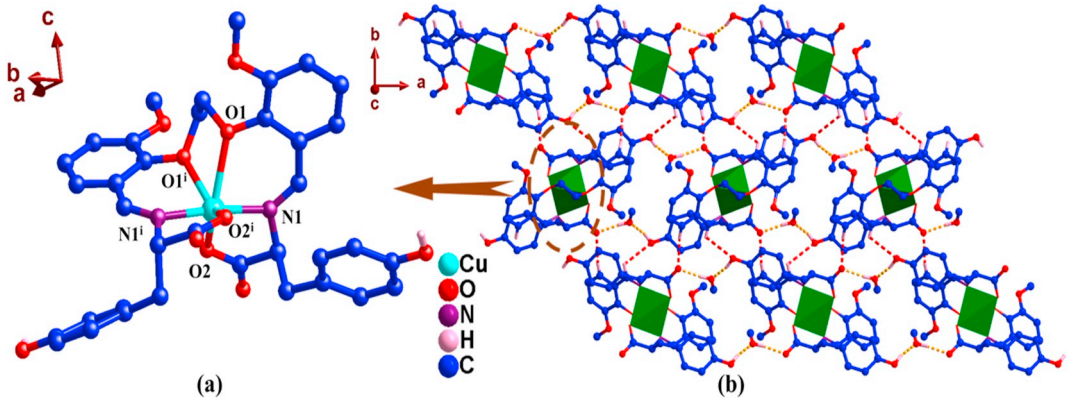

Fig. 3. The molecular structure (a) and the 2-D layer structure (b) of [Cu($C_{36}H_{34}N_2O_{10}$)]·2CH_3OH (**3**), which constructed by O—H···O hydrogen bonds (yellow dash bonds) and C—H···O interactions (red dash bonds).

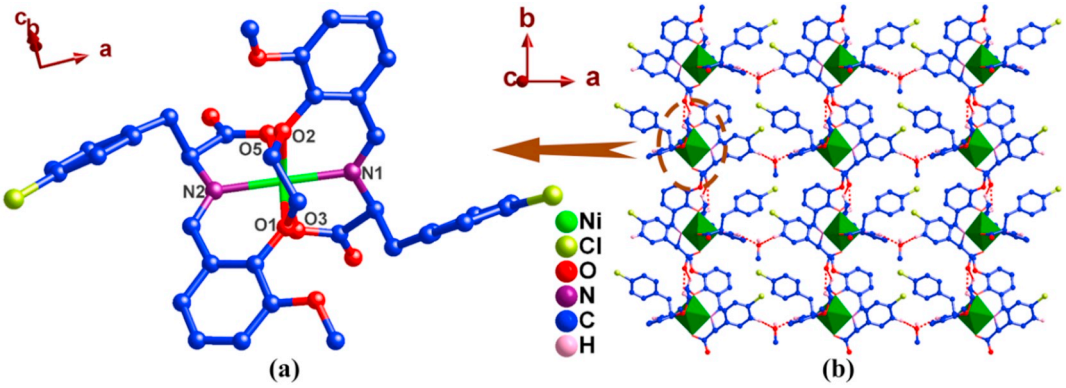

Fig. 4. The molecular structure (a) and the 2-D layer structure (b) of $[Ni(C_{36}H_{32}N_2O_8Cl_2)]\cdot 2CH_3OH$ (**4**), which constructed by C—H···O interactions (red dash bonds).

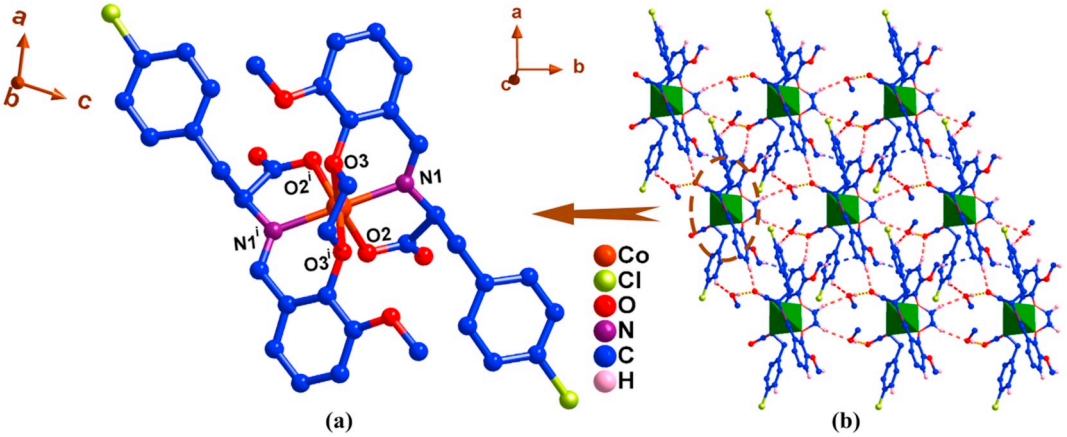

Fig. 5. The molecular structure (a) and the 2-D layer structure (b) of $[Co(C_{36}H_{32}N_2O_8Cl_2)]\cdot 4CH_3OH$ (**5**), which constructed by O—H···O hydrogen bonds (yellow dash bonds) and C—H···O interactions (red dash bonds).

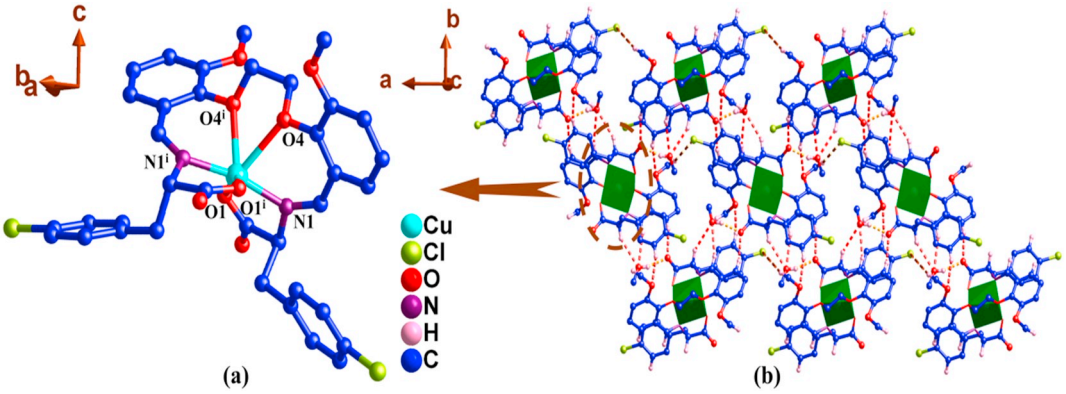

Fig. 6. The molecular structure (a) and the 2-D layer structure (b) of $[Cu(C_{36}H_{32}N_2O_8Cl_2)]\cdot 2CH_3OH$ (**6**), which constructed by O—H···O hydrogen bonds (yellow dash bonds), C—H···O interactions (red bonds) and C—H···Cl interactions (dark-red dash bonds).

while that of LEU839 N-H···$O_{complex\text{-}6}$ are 2.224 Å and 164.1°. At the same time, complex **6** formed π-π stacking interaction with the said chain benzene ring of amino-acid residue PHE712, σ-π interaction with the C atom of amino-acid residue PHE838, with the distances of the interactions being 5.245 and 3.757 Å respectively (Fig. 10a).

In the inhibitor-urease complex conformation, the Cu(II) complexes **3** and **6** showed a more stabilized structure than the corresponding Ni (II) complexes **1** and **4**. The docking structures of complexes **3** and **6** are overlayed with the geometrically optimized structures, and it is found that the superposition is good, except for a certain degree of spatial change of the side groups (Fig. 11). This result satisfies the principle of spatial geometric complementarity. The percentages of highest occupied molecular orbital (HOMO) of carboxyl O atoms in the optimized structures of Cu(II) complexes **3** (21.72%, 27.27%) and **6** (30.32%, 22.53%) are obviously much higher than the corresponding values observed in the Ni(II) and Co(II) complexes **1** (2.70%, 0.31%), **2** (8.96%, 8.18%), **4** (5.91%, 7.42%) and **5** (9.61%, 9.64%) (Fig. S16). Therefore, these O atoms in complexes **3** and **6** are much more easier to give electrons and are much more easier to be recognized by amino-acid residue of urease. This result can reasonably explain the difference in urease inhibitory activity between the Cu(II) complex and the same series of Ni(II), Co(II) complexes with the same ligand from the perspective of theoretical calculation. And after docking, the values of E_{HOMO} of complexes **3** and **6** increased (−5.687 eV to −5.442 eV;

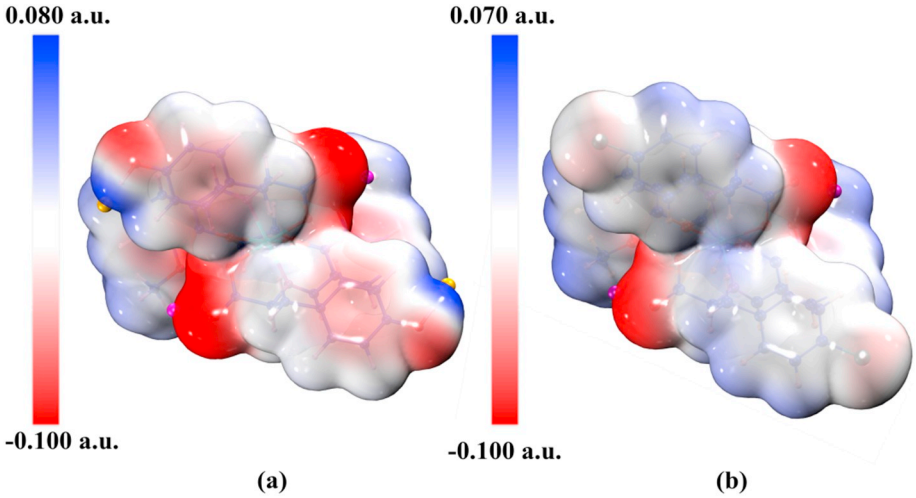

Fig. 7. The total electron density mapped with electrostatic surface of complexes **3** and **6** (mapped into the electron density isosurface of 0.001 electrons/au^3). The yellow ball corresponds to the maximum point of the electrostatic potential, and the magenta ball corresponds to the minimum electrostatic potential.

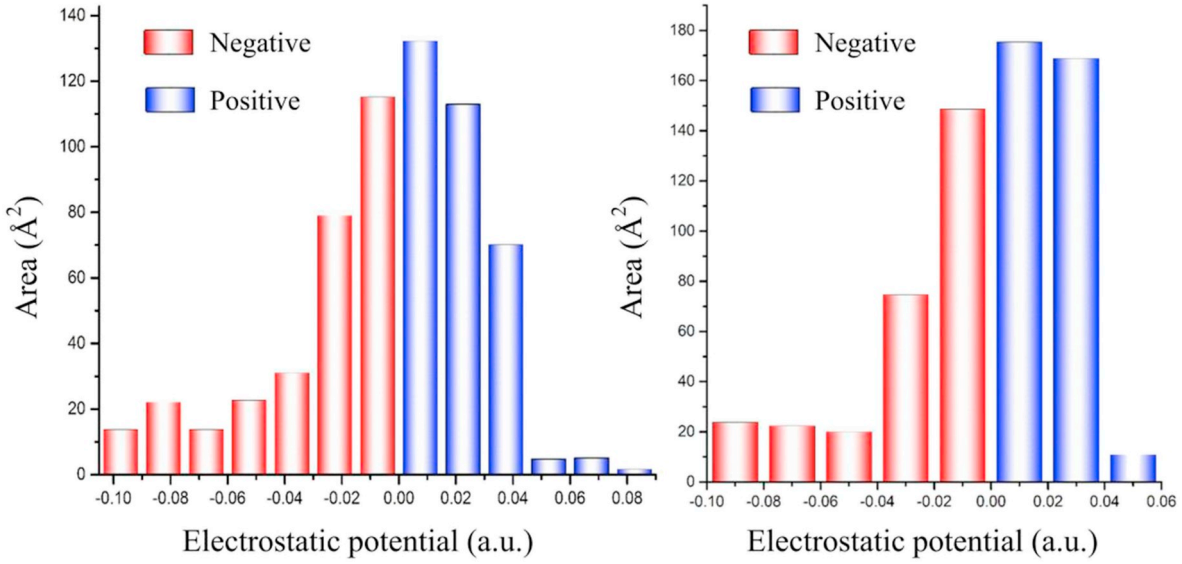

Fig. 8. The MEP interval distributions of complexes **3** and **6**.

Table 3
Inhibition of jack bean urease by Schiff base ligands and complexes **1–6**.

Tested materials	IC_{50} (μM)
H_2L_{1-2}	> 100
Complex **1**	20.43 ± 1.26
Complex **2**	26.01 ± 2.35
Complex **3**	10.36 ± 1.13
Complex **4**	30.52 ± 3.12
Complex **5**	36.41 ± 1.56
Complex **6**	15.63 ± 3.04
Acetohydroxamic acid[a]	26.99 ± 1.43

[a] Used as a positive control.

−5.903 eV to −5.692 eV) (Fig. S17, Fig. S18), and the percentages of HOMO of the carboxyl O atoms further increased slightly (Fig. S16).

Compared binding modes of all four complexes, complex **3**, as a guest molecule, is well embedded into the active pocket of jack bean urease through three types of hydrogen bonds interactions mentioned above, including the O−H···O_{SER421} hydrogen bond interaction formed between the 4-hydroxyphenyl pendant group in complex **3** and the amino-acid residue SER421. In contrast, no hydrogen bond was found between 4-chlorophenyl pendant group in complex **6** and the amino acid residues of the urease active site. At the same time, the spatial steric hindrance of the 4-chlorophenyl pendant group is relatively higher than that of the 4-hydroxyphenyl pendant group in complex **3**. This probably causes the activity difference of complexes **3** and **6** as urease inhibitors. In addition, the affinity energy (−41.42 kJ/mol) in the modeled structure of **3**-urease complex is slightly lower than the corresponding value (−39.33 kJ/mol) observed in the **6**-urease complex. The results further demonstrate the certain degree of difference of urease inhibitory activity of these two Cu(II) complexes.

4. Conclusion

In summary, the present paper has reported the synthesis, crystal structures, DFT calculations and urease inhibition properties of two different series of Ni(II), Co(II) and Cu(II) complexes with sexidentate N_2O_4-donor bis-Schiff base ligand. It was found that complexes **3** (IC_{50} = 10.36 ± 1.13 μM) and **6** (IC_{50} = 15.63 ± 3.04 μM) possess the good inhibitory activities again jack bean urease. Moreover, the structure-inhibitory activity relationship of complex **1–6** was further

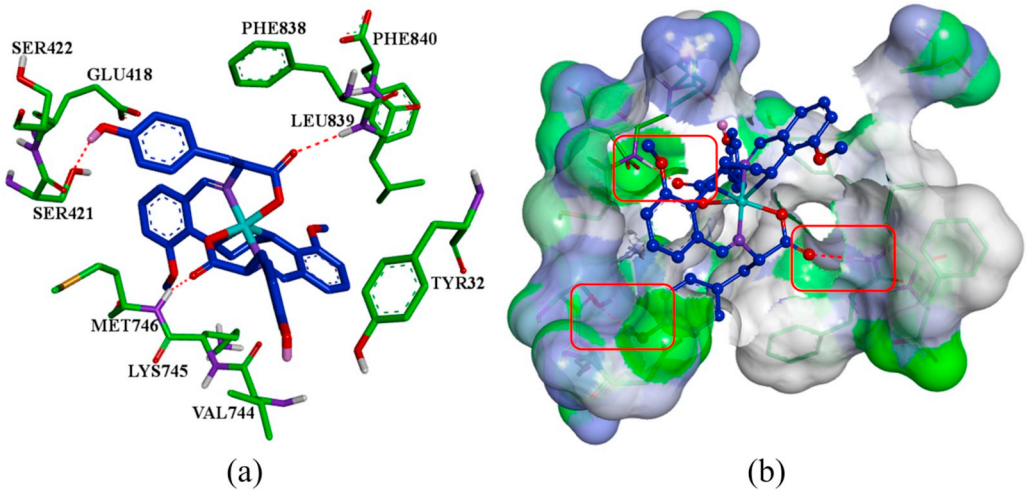

Fig. 9. The modeled structure (a) of urease-inhibitor complex **3**, N—H···O hydrogen bond interaction and O—H···O hydrogen bond interaction are presented as red dash lines. Binding mode (b) of complex **3** with jack bean urease. The enzyme is shown as surface and the complex is shown as sticks.

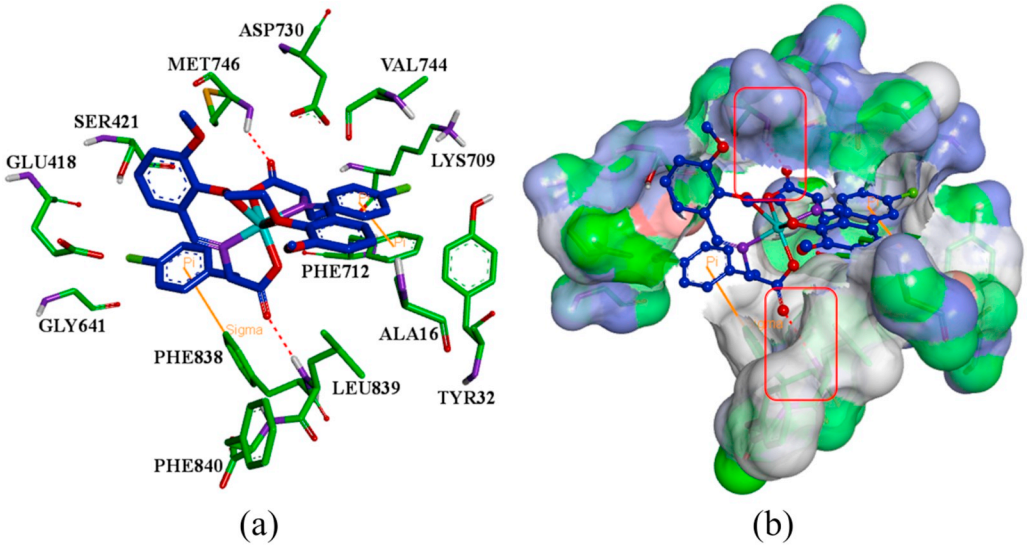

Fig. 10. The modeled structure (a) of urease-inhibitor complex **6**, N—H···O hydrogen bond interaction, π-π stacking interaction and σ-π interaction are presented as red dash lines and yellow lines. Binding mode (b) of complex **6** with jack bean urease. The enzyme is shown as surface and the complex is shown as sticks.

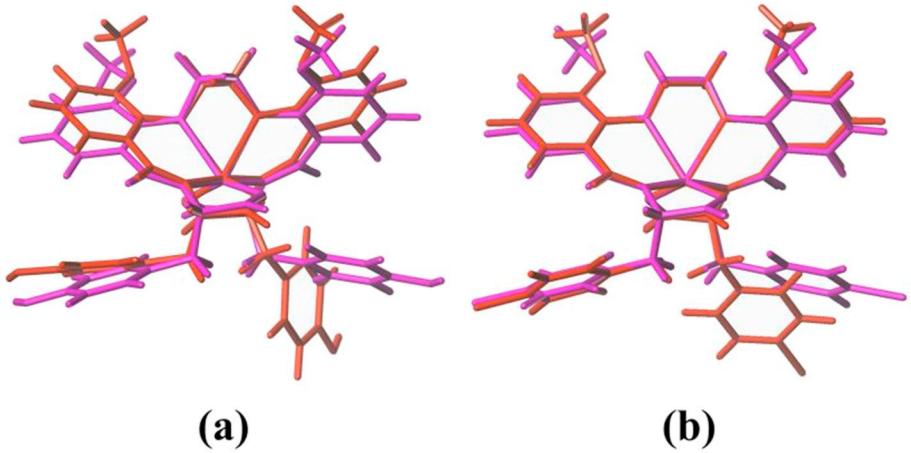

Fig. 11. The superposition of optimized (fuchsia) and docking structures (red) of complexes **3** (a) and **6** (b).

discussed from the perspective of molecular docking and theoretical calculation, suggesting that the Cu(II) complexes **3** and **6** have good potential as the urease inhibitor in the future. Theoretical calculation results showed a good accordance between experimental and calculated results. Detailed investigations are continuing to study the mechanisms of urease inhibitory activity reported here.

Acknowledgments

This research was supported by the National Natural Science Foundation of China to C.F. Bi (No. 21371161), the Specialized Research Fund for the Doctoral Program of Higher Education of China to Y.H. Fan (No. 20120132110015)

Appendix A. Supplementary data

Crystallographic information of three complexes have been deposited with the Cambridge Crystallographic Data Center as supplementary publication CCDC No. 1525034 (for **1**), No. 1848911 (for **2**), No. 1559238 (for **3**), No. 1841584 (for **4**), No. 1842892 (for **5**), No. 1844678 (for **6**). Copies of the data may be obtained free of charge on application to CCDC, 12 Union Road, Cambridge CB2 1EB, UK (Fax: +44-1223-336-033; E-mail: deposit@ccdc.cam.ac.uk or http://www.ccdc.cam.ac.uk). Supplementary data to this article can be found online at https://doi.org/10.1016/j.jinorgbio.2019.110959.

References

[1] X.C. Shi, H.B. Fang, Y. Guo, H. Yuan, Z.J. Guo, X.Y. Wang, J. Inorg. Biochem. 190 (2019) 38–44.
[2] X.X. Wang, M.L. Zhu, F. Gao, Y. Qian, H.K. Liu, J. Zhao, J. Inorg. Biochem. 180 (2018) 179–185.
[3] T. Marzo, F. Navas, D. Cirri, A. Merlino, G. Ferraro, L. Messori, A.G. Quiroga, J. Inorg. Biochem. 181 (2018) 11–17.
[4] J.P. Liu, C. Zhang, T.W. Rees, L.B. Ke, L.N. Ji, H. Chao, Coordin. Chem. Rev. 363 (2018) 17–28.
[5] D.G. Diana, C. Diana, P. Yolanda, C. Paula, D.H. Isabel, P. Sanjiv, F.F. Eva, G.R. Santiago, Dalton Trans. 47 (2018) 12284–12299.
[6] S. Medici, M. Peana, V.M. Nurchi, J.I. Lachowicz, G. Crisponi, M.A. Zoroddu, Coordin. Chem. Rev. 284 (2015) 329–350.
[7] A. Cuprys, R. Pulicharla, S.K. Brar, P. Drogui, M. Verma, R.Y. Surampalli, Coordin. Chem. Rev. 376 (2018) 46–61.
[8] E. Viñuelas-Zahínos, F. Luna-Giles, P. Torres-García, M.C. Fernández-Calderón, Eur. J. Med. Chem. 46 (2011) 150–159.
[9] T.R. Lakshman, J. Deb, I. Ghosh, S. Sarkar, T.K. Paine, Inorg. Chim. Acta 486 (2019) 663–668.
[10] U. Kendur, G.H. Chimmalagi, S.M. Patil, K.B. Gudasi, C.S. Frampton, C.V. Mangannavar, I.S. Muchchandi, J. Mol. Struct. 1153 (2018) 299–310.
[11] X. Yu, M.C. Chau, W.K. Tang, C.K. Siu, Z.P. Yao, Anal. Chem. 90 (2018) 4089–4097.
[12] T.S. Reddy, S.H. Privér, N. Mirzadeh, S.K. Bhargava, Eur. J. Med. Chem. 145 (2018) 291–301.
[13] B. Demoro, S. Rostán, M. Moncada, Z.H. Li, R. Docampo, C. Olea Azar, J.D. Maya, J. Torres, D. Gambino, L. Otero, J. Biol. Inorg. Chem. 23 (2018) 303–312.
[14] M.E.K. Stathopoulou, C.N. Banti, N. Kourkoumelis, A.G. Hatzidimitriou, A.G. Kalampounias, S.K. Hadjikakou, J. Inorg. Biochem. 181 (2018) 41–55.
[15] P. Mandal, B.K. Kundu, K. Vyas, V. Sabu, A. Helen, S.S. Dhankhar, C.M. Nagaraja, D. Bhattacherjee, K.P. Bhabak, S. Mukhopadhyay, Dalton Trans. 47 (2018) 517–527.
[16] L. Habala, F. Devínsky, A.E. Egger, J. Coord. Chem. 71 (2018) 907–940.
[17] M.H. Alqarni, M.M. Muharram, N.E. Labrou, Int. J. Biol. Macromol. 116 (2018) 84–90.
[18] L. Zhang, P. Carroll, E. Meggers, Org. Lett. 6 (2004) 521–523.
[19] H. Bregman, D.S. Williams, G.E. Atilla, P.J. Carroll, E. Meggers, J. Am. Chem. Soc. 126 (2004) 13594–13595.
[20] D. Majumdar, D. Das, S.S. Sreejith, S. Das, J. Kumar Biswas, M. Mondal, D. Ghosh, K. Bankura, D. Mishra, Inorg. Chim. Acta 489 (2019) 244–254.
[21] Y. Lin, W. An, X. Ge, M. Liu, Y. Wang, X. Liu, L. Tian, J. Coord. Chem. 72 (2019) 987–1001.
[22] M. Murugaiyan, S.P. Mani, M.A. Sithique, New J. Chem. 43 (2019) 9540–9554.
[23] M.T. Kaczmarek, M. Zabiszak, M. Nowak, R. Jastrzab, Coord. Chem. Rev. 370 (2018) 42–54.
[24] R. Gueret, C.E. Castillo, M. Rebarz, F. Thomas, M. Sliwa, J. Chauvin, B. Dautreppe, J. Pécaut, J. Fortage, M.N. Collomb, Inorg. Chem. 58 (2019) 9043–9056.
[25] S. Dharani, G. Kalaiarasi, D. Sindhuja, V.M. Lynch, R. Shankar, R. Karvembu, R. Prabhakaran, Inorg. Chem. 58 (2019) 8045–8055.
[26] S.L. Hooe, A.L. Rheingold, C.W. Machan, J. Am. Chem. Soc. 140 (2018) 3232–3241.
[27] A.N. Gusev, M.A. Kiskin, E.V. Braga, M. Chapran, G. Wiosna-Salyga, G.V. Baryshnikov, V.A. Minaeva, B.F. Minaev, K. Ivaniuk, P. Stakhira, H. Ågren, W. Linert, J. Phys. Chem. C 123 (2019) 11850–11859.
[28] J. Zhao, F. Dang, B. Liu, Y. Wu, X. Yang, G. Zhou, Z. Wu, W.Y. Wong, Dalton Trans. 46 (2017) 6098–6110.
[29] M. Karmakar, S. Roy, S. Chattopadhyay, New J. Chem. 43 (2019) 10093–10102.
[30] L. Rigamonti, A. Forni, S. Righetto, A. Pasini, Dalton Trans. 48 (2019) 11217–11234.
[31] S.M. Borisov, R. Pommer, J. Svec, S. Peters, V. Novakova, I. Klimant, J. Mater. Chem. C 6 (2018) 8999–9009.
[32] J. Zhang, L. Xu, W.Y. Wong, Coord. Chem. Rev. 355 (2018) 180–198.
[33] R.A. Burne, Y.Y.M. Chen, Microb. Infect. 2 (2000) 533–542.
[34] C. Follmer, J. Clin. Pathol. 63 (2010) 424–430.
[35] I. Konieczna, P. Zarnowiec, M. Kwinkowski, B. Kolesinska, J. Fraczyk, Z. Kaminski, W. Kaca, Curr. Protein Pept. Sci. 13 (2012) 789–806.
[36] M.A. Zaheer-ul-Haq, S.A. Lodhi, S. Nawaz, Iqbal, K.M. Khan, et al., Bioorg. Med. Chem. 16 (2008) 3456–3461.
[37] H.Q. Li, C. Xu, H.S. Li, L. Shi, Z.P. Xiao, H.L. Zhu, ChemMedChem 2 (2007) 1361–1369.
[38] T. Tanaka, M. Kawase, S. Tani, Life Sci. 73 (2003) 2985–2990.
[39] L. Mazzei, M. Cianci, U. Contaldo, S. Ciurli, J. Agric. Food Chem. 67 (2019) 2127–2138.
[40] C. Samorì, L. Mazzei, S. Ciurli, G. Cravotto, G. Grillo, E. Guidi, A. Pasteris, S. Tabasso, P. Galletti, ACS Sustain. Chem. Eng. 7 (2019) 15558–15567.
[41] V. Ntatsopoulos, K. Macegoniuk, A. Mucha, S. Vassiliou, L. Berlicki, Eur. J. Med. Chem. 159 (2018) 307–316.
[42] M. Taha, H. Ullah, L.M.R. Al Muqarrabun, M.N. Khan, F. Rahim, N. Ahmat, M.T. Javid, M. Ali, K.M. Khan, Bioorgan. Med. Chem. 26 (2018) 152–160.
[43] L. Pan, C.F. Wang, K.D. Yan, K. Zhao, G.H. Sheng, H.L. Zhu, X.L. Zhao, D. Qu, F. Niu, Z.L. You, J. Inorg. Biochem. 159 (2016) 22–28.
[44] Y.M. Li, L. Xu, M.M. Duan, B.T. Zhang, Y.H. Wang, Y.X. Guan, J.H. Wu, C.L. Jing, Z.L. You, Polyhedron. 166 (2019) 146–152.
[45] X.X. Chen, C.Y. Wang, J.J. Fu, Z.W. Huang, Y.Y. Xu, S.Q. Wang, Inorg. Chem. Commun. 99 (2019) 70–76.
[46] H. Wang, T.X. Lan, X. Zhang, D.M. Zhang, C.F. Bi, Y.H. Fan, J. Inorg. Biochem. 165 (2016) 18–24.
[47] H. Tuncer, Ç. Erk, Dyes Pigments 44 (2000) 81–86.
[48] G.M. Sheldrick, Acta. Crystallographica. C. C71 (2015) 3–8.
[49] S.M.A.R.T. Bruker, Version 5.0, SAINT-Plus Version 6, SHELXTL, Version 6.1, SADABS Version 2.03, Bruker AXS Inc, Madison, WI, 2000.
[50] A.D. Becke, J. Chem. Phys. 98 (1993) 5648–5653.
[51] C. Lee, W. Yang, R.G. Parr, Phys. Rev. B. Matter. 37 (1988) 785–789.
[52] J.M. Seminario, Advances in Quantum Chemistry, Density Functional Theory, Academic Press, New York, 1998.
[53] P.J. Hay, W.R. Wadt, J. Chem. Phys. 82 (1985) 299–310.
[54] K.D. Frisch, G.W. Trucks, H.B. Schlegel, M.A. Robb, et al., Gaussian 03, Revision A. 6, Gaussian, Inc, Pittsburgh PA, 2003.
[55] T. Tanaka, M. Kawase, S. Tani, Life Sci. 73 (2003) 2985–2990.
[56] W. Zaborska, B. Krajewska, Z. Olech, J. Enzyme. Inhib. Med. Chem. 19 (2004) 65–69.
[57] D.D. Van Slyke, R.M. Archibald, J. Biol. Chem. 154 (1944) 623–642.
[58] O. Trott, A.J. Olson, J. Comput. Chem. 31 (2010) 455–461.
[59] H. Wang, X. Zhang, Y. Zhao, D.M. Zhang, F. Jin, Y.H. Fan, Inorg. Chim. Acta 466 (2017) 8–15.
[60] H. Wang, X. Zhang, Y. Zhao, D.M. Zhang, F. Jin, Y.H. Fan, J. Mol. Struct. 1148 (2017) 496–504.
[61] N. Okulik, A.H. Jubert, Internet Electron. J. Mol. Des. 4 (2005) 17–30.
[62] P. Politzer, P.R. Laurence, K. Jayasuriya, J. McKinney, Environ. Health Perspect. 61 (1985) 191–202.
[63] T. Lu, F.W. Chen, J. Comput. Chem. 33 (2012) 580–592.
[64] T. Lu, F.W. Chen, J. Mol. Graph. Model. 38 (2012) 314–323.
[65] W.H.R. Shaw, D.N. Raval, J. Am. Chem. Soc. 83 (1961) 3184–3187.
[66] X.W. Dong, Y.G. Li, Z.W. Li, Y.M. Cui, H.L. Zhu, J. Inorg. Biochem. 108 (2012) 22–29.
[67] X.W. Dong, T.L. Guo, Y.G. Li, Y.M. Cui, Q. Wang, J. Inorg. Biochem. 127 (2013) 82–89.